ARTICLES
PUBLISHED ONLINE: 6 FEBRUARY 2017 | DOI: 10.1038/NPHYS4027
nature physics

State-resolved attosecond reversible and irreversible dynamics in strong optical fields

Mazyar Sabbar[1*†], Henry Timmers[1†], Yi-Jen Chen[2,3†], Allison K. Pymer[4], Zhi-Heng Loh[5], Scott G. Sayres[6,7], Stefan Pabst[8,9], Robin Santra[2,3] and Stephen R. Leone[1,10,11*]

Strong-field ionization (SFI) is a key process for accessing real-time quantum dynamics of electrons on the attosecond timescale. The theoretical foundation of SFI was pioneered in the 1960s, and later refined by various analytical models. While asymptotic ionization rates predicted by these models have been tested to be in reasonable agreement for a wide range of laser parameters, predictions for SFI on the sub-laser-cycle timescale are either beyond the scope of the models or show strong qualitative deviations from full quantum-mechanical simulations. Here, using the unprecedented state specificity of attosecond transient absorption spectroscopy, we follow the real-time SFI process of the two valence spin–orbit states of xenon. The results reveal that the irreversible tunnelling contribution is accompanied by a reversible electronic population that exhibits an observable spin–orbit-dependent phase delay. A detailed theoretical analysis attributes this observation to transient ground-state polarization, an unexpected facet of SFI that cannot be captured by existing analytical models that focus exclusively on the production of asymptotic electron/ion yields.

Ionization in the presence of a strong laser field can occur either through a multiphoton-mediated process, where the missing energy to surpass the ionization barrier is provided by the simultaneous absorption of multiple photons, or by tunnelling through a field-induced potential barrier when the laser electric field significantly alters the atomic potential. The relative contribution of the two pathways to strong-field ionization (SFI) is commonly classified by the Keldysh parameter[1] $\gamma = \omega_L\sqrt{2I_p m_e}/(eE_L)$, where ω_L is the frequency of the laser, I_p is the ionization potential, E_L is the laser electric field and e, m_e are the charge and mass of the electron, respectively. The concept is based on the time the electron needs to tunnel through the combined Coulomb–laser potential barrier. For a low-frequency laser field with high intensities ($\gamma \ll 1$), the ionization process can be regarded as quasi-static, giving the electron enough time to overcome the field-induced barrier before the potential significantly changes. In this regime, referred to as adiabatic SFI, tunnelling dominates over multiphoton ionization. Conversely, in the limit of high frequencies and low intensities ($\gamma \gg 1$), tunnelling is suppressed by the decreased tunnelling time window and the increased barrier width. In this regime, referred to as non-adiabatic SFI, ionization by the absorption of several photons is favoured. A vast number of experiments[2–5] have been performed to study SFI in both regimes by measuring the asymptotic momentum distribution or the yield of freed electrons/ions upon ionization by a strong laser field. While these experiments provide evidence for the justification of various theoretical approaches, it is paramount to access the real-time dynamics of the ionization process to gain a more comprehensive understanding of SFI. Since conventional strong-field laser systems have optical periods corresponding to a few femtoseconds, it is necessary to apply attosecond techniques to probe the sub-cycle ionization mechanisms.

From its initial realization, attosecond spectroscopy[6,7] has revolutionized time-resolved methods by fully capturing the dynamics of quantum systems ranging from nuclear motion within molecules and solids to more elusive dynamics of the constituent electrons in atoms, molecules and solid-state devices. In the past decade, attosecond spectroscopy has been extensively applied to study electronic motion in real time, including the observation of a few-femtosecond Auger process[6], unexpected ionization delays between electronic sub-shells in solid-state materials[7,8] and atoms[9–11], and the first experimental evidence for ionization steps in field-induced tunnel ionization[12]. In more recent years, attosecond pulses have also been combined with the transient absorption technique[13–15]. This method probes the dynamics directly in the pump–probe interaction volume and tracks the occurrence of these dynamics through state-selected internal transitions. Following this route, Wirth *et al.*[16] presented a study on the time dynamics of SFI in atomic Kr using a sub-cycle ionizing field. They were able to observe sub-femtosecond ionization confinement allowing them to launch a valence wavepacket with very high coherence. However, owing to the low polarizability of Kr ($\alpha_0^{Kr} \approx 17$ a.u.)[17,18] and statistical errors, sub-cycle effects during SFI could not be clearly resolved, thus preventing a comprehensive interpretation of the SFI process.

In the study presented here, the sensitivity of attosecond transient absorption spectroscopy (ATAS) is used to systematically probe

[1]Department of Chemistry, University of California, Berkeley, California 94720, USA. [2]Center for Free-Electron Laser Science, DESY, D-22607 Hamburg, Germany. [3]Department of Physics, University of Hamburg, D-20355 Hamburg, Germany. [4]Eastman Chemical Company, Kingsport, Tennessee 37660, USA. [5]Division of Chemistry and Biological Chemistry, and Division of Physics and Applied Physics, School of Physical and Mathematical Sciences, and Centre for Optical Fibre Technology, The Photonics Institute, Nanyang Technological University, Singapore 639798, Singapore. [6]School of Molecular Sciences, Arizona State University, Tempe, Arizona 85287, USA. [7]Biodesign Center for Applied Structural Discovery, Arizona State University, Tempe, Arizona 85287, USA. [8]ITAMP, Harvard-Smithsonian Center for Astrophysics, Cambridge, Massachusetts 02138, USA. [9]Physics Department, Harvard University, Cambridge, Massachusetts 02138, USA. [10]Chemical Sciences Division, Lawrence Berkeley National Laboratory, Berkeley, California 94720, USA. [11]Department of Physics, University of California, Berkeley, California 94720, USA. [†]These authors contributed equally to this work.
*e-mail: mazyar.sabbar@gmail.com; srl@berkeley.edu

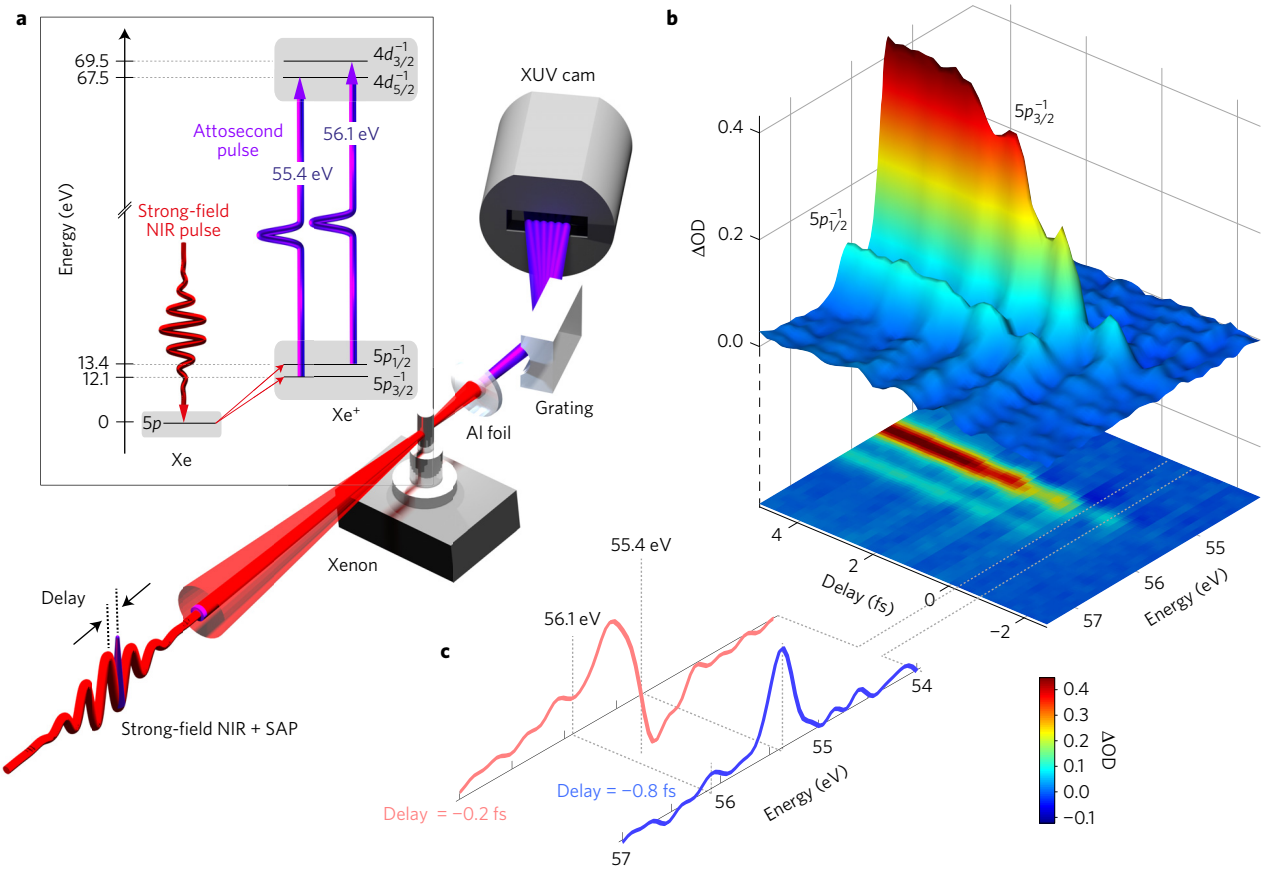

Figure 1 | Experimental scheme and results. a, An intense waveform-stabilized, few-cycle near-infrared (NIR) laser pulse (red) induces SFI in Xe atoms, which creates a hole population in the spin-orbit split states, $5p_{1/2}^{-1}$ and $5p_{3/2}^{-1}$ of the emerging ions. A time-delayed single attosecond pulse (purple) is used to probe the population in both of the states by promoting the valence holes into the $4d_{3/2}^{-1}$ and $4d_{5/2}^{-1}$ core states. The dynamics are recorded by measuring the transient changes in the spectrum of the single attosecond pulse by means of an extreme ultraviolet (XUV) spectrometer. **b**, Transient absorption spectra measured as a function of the delay between the NIR and isolated attosecond pulse for a NIR intensity of 3.2×10^{14} W cm^{-2}. The upper panel shows a surface representation underlining the observation of half-cycle overshoots, whereas the projection depicted in the lower panel emphasizes changes in the lineshape. **c**, Snapshots of the spectrum for two different delays at which the lineshape changes most drastically.

real-time, strong-field-induced dynamics in the valence spin–orbit states of Xe ions. Due to its high static ground-state polarizability ($\alpha_0^{Xe} \approx 27$ a.u.)[17,18], Xe serves as an ideal experimental test system to study not only the response of valence electrons that results in irreversible ionization but also the temporary displacement of bound electrons giving rise to polarization. Indeed, numerical calculations[19,20], based on solving the time-dependent Schrödinger equation, consistently predict strong polarization effects for Keldysh parameters accessible in experimental set-ups ($\gamma \approx 1$). In this study, the strong-field interaction process is followed in real time and the first experimental evidence is observed for such ultrafast field-induced polarization effects in a channel-resolved manner. The results are in excellent agreement with theoretical calculations obtained from the time-dependent configuration interaction singles (TDCIS) method[21–23], a first-principles approximation scheme for solving the many-electron time-dependent Schrödinger equation in full spatial dimensionality, systematically taking into consideration competing ionization channels.

Experiment and observations

The principles of the ATAS experimental scheme are presented in Fig. 1a. A few-cycle, waveform-stabilized near-infrared (NIR) pulse centred around 790 nm is focused into a cell filled with Xe gas. The interaction of the strong laser field with the Xe atoms results in the ionization of Xe to the two valence spin–orbit states, $5p_{1/2}^{-1}$ and $5p_{3/2}^{-1}$. The peak intensity of the NIR pulse is varied between 2.0×10^{14} and 3.2×10^{14} W cm^{-2}, corresponding to Keldysh parameters of $\gamma \approx 0.72$ and 0.57, respectively. The ionization is therefore expected to be dominated by a tunnelling type mechanism. To probe the creation of Xe^+, a time-delayed isolated attosecond pulse centred at near 60 eV is used to excite the $5p_{1/2}^{-1}$ and $5p_{3/2}^{-1}$ valence holes to the $4d$ inner shell. The transitions introduce characteristic absorption lines in the spectrum of the attosecond pulse at 55.4 eV and 56.1 eV, corresponding to the two strongest hole transitions $5p_{3/2}^{-1} \rightarrow 4d_{5/2}^{-1}$ and $5p_{1/2}^{-1} \rightarrow 4d_{3/2}^{-1}$, respectively. At the intensities applied in this study, the third dipole-allowed transition corresponding to $5p_{3/2}^{-1} \rightarrow 4d_{3/2}^{-1}$ does not provide a sufficiently high signal-to-noise ratio to enable the observation of attosecond ionization dynamics. The interaction of the strong NIR laser field with Xe atoms is captured by recording the transient absorption spectrum defined by the differential optical density, or $\Delta\mathrm{OD}(E,\tau) = -\ln[I_{on}(E,\tau)/I_{off}(E,\tau)]$, as a function of the time delay τ between the NIR-pump and extreme ultraviolet (XUV)-probe pulses. Here, I_{on} and I_{off} represent the XUV spectra with and without the NIR-pump field. For given target parameters, ΔOD is directly proportional to the absorption cross-section, which gives access to the real-time valence-hole population[24]. The results of the ATAS experiment for an intensity of 3.2×10^{14} W cm^{-2} are shown in Fig. 1b.

The data contain rich spectroscopic features for both of the spin–orbit channels imprinted by the underlying strong-field dynamics. Most importantly, the attosecond temporal resolution provides access to the natural timescale of the dynamics dictated by

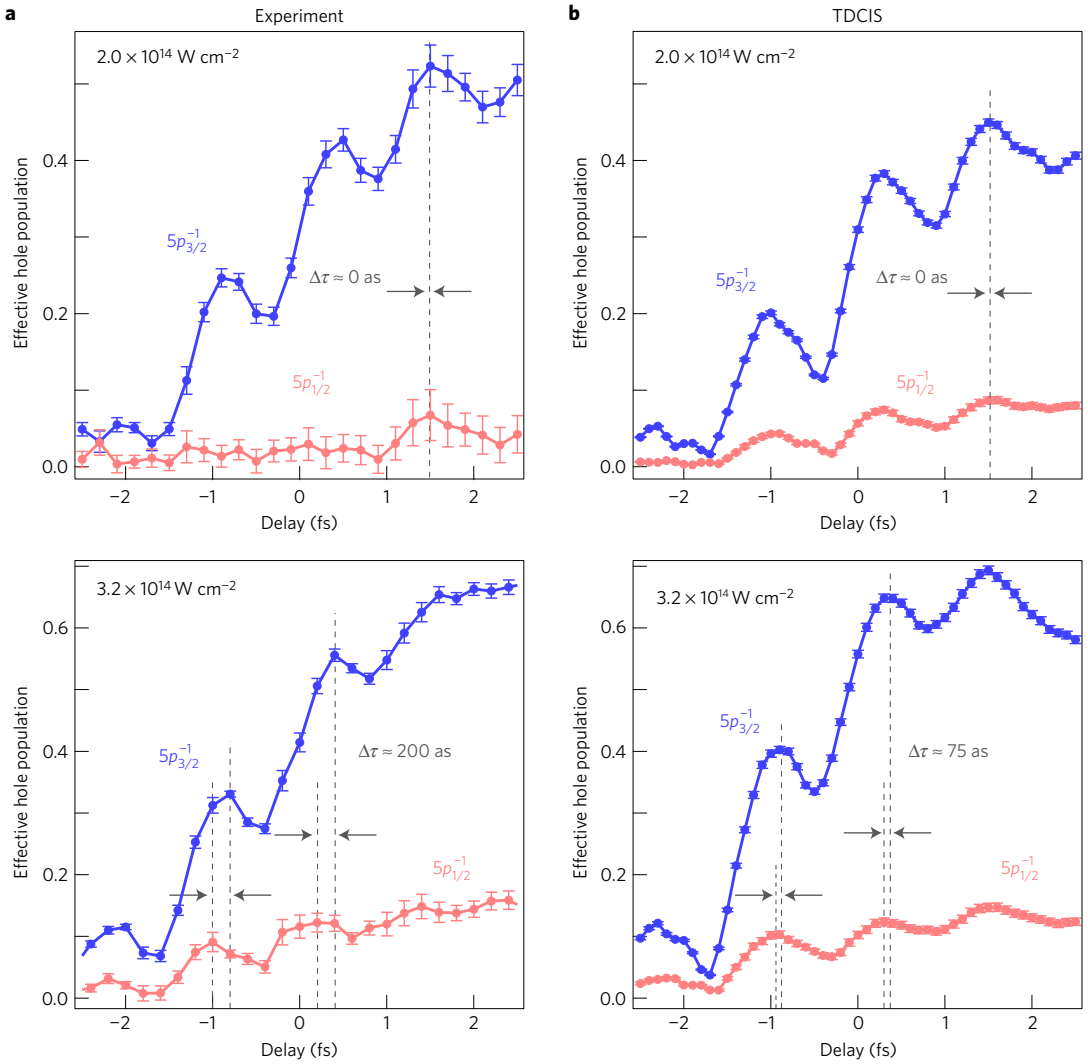

Figure 2 | Reconstructing experimental and theoretical effective Xe^+ populations from ATAS spectrograms. a,**b**, A fitting procedure on the ATAS spectrogram based on the oscillating dipole model allows for the reconstruction of the ionic populations in the $5p_{1/2}^{-1}$ (red) and $5p_{3/2}^{-1}$ (blue) states for the experimental (**a**) and theoretical (**b**) data sets. For a more direct comparison between experimental and TDCIS data sets, the unknown offsets of the delay axes of the experimental data in **a** have been shifted by +0.5 fs and −1.2 fs for the intensities of 2.0×10^{14} W cm^{-2} and 3.2×10^{14} W cm^{-2}, respectively. The trends in oscillation strengths and relative phases of the two ionization channels for both intensities demonstrate the solid agreement between experiment and the TDCIS method. For the evaluation of the relative phase delays, we consider only the overshoot positions where the experimental SFI dynamics provide enough signal to noise and display noticeable oscillations. The error bars on the data represent the 95% confidence interval resulting from the fitting procedure.

the strong laser field. As can be observed, in both of the spin–orbit states, ionization occurs with a characteristic step-like behaviour, providing strong evidence for the tunnelling nature of the measured process. As expected from both adiabatic[1,25,26] and non-adiabatic[27] SFI theories, tunnelling mainly follows the oscillating laser field in a nonlinear fashion. Thus, particularly around the nodes of the electric field, the ionic population is expected to form plateaux. However, both spin–orbit channels observed in Fig. 1b exhibit pronounced maxima that occur with a periodicity of 1.2 fs, which coincides with twice the laser frequency ω_L. This deviation from the expected plateau structure will henceforth be referred to as overshoots. As will be demonstrated with the aid of theory, the overshoots are a direct signature of bound electron motion. A deeper look into the measured spectrogram also reveals strong periodic line deformations at $2\omega_L$ frequency (Fig. 1c). Consequently, the population dynamics cannot be extracted directly from a simple lineout analysis. As has been demonstrated in previous experiments[16,24,28], such NIR-induced lineshape modifications can be understood within an oscillating dipole model[24]. The coherent superposition of the $5p^{-1}$ and $4d^{-1}$ states created by the XUV pulse generates an oscillating ionic dipole that decays with some characteristic lifetime due to the Auger decay of the $4d^{-1}$ hole ($\tau_{Auger} \approx 6$fs; ref. 29). Provided that the dipole subsequently undergoes field-free evolution, this decay will lead to a characteristic Lorentzian absorption profile. However, when the NIR and XUV pulses temporally overlap—as is the case in the experiment—the NIR pulse can still perturb the oscillating dipole before it damps out, leading to a phase shift in the dipole and giving rise to an asymmetric, Fano absorption profile.

Effective hole dynamics and theory comparison

To extract the time-dependent electron–hole populations and dipole phase modifications in the presence of lineshape modifications, we apply a fitting procedure based on the oscillating dipole model[24] (for details see Supplementary Sections 1.3 and 2.1). Figure 2a presents the effective hole populations (EHPs) extracted from the experimental ATAS data, which are proportional to the fitting

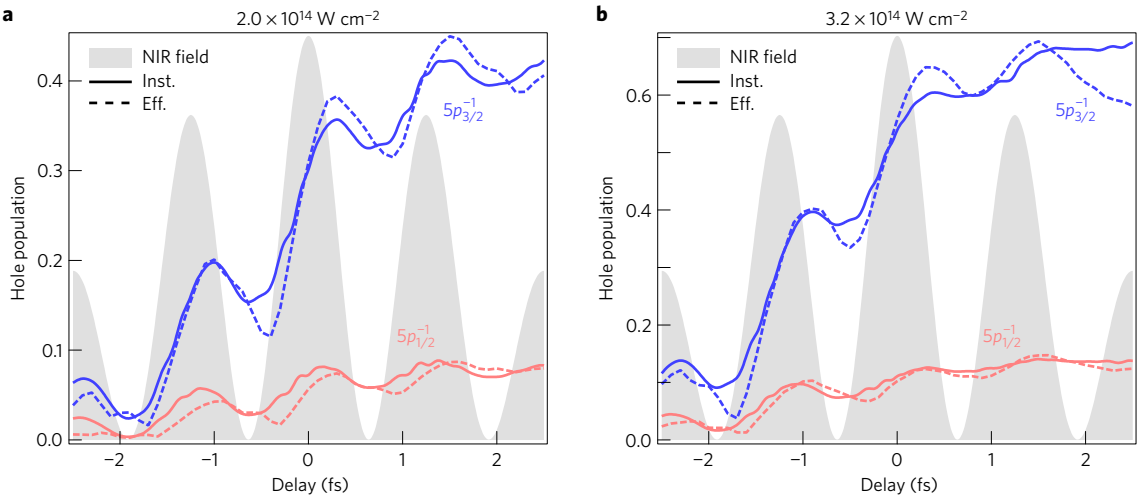

Figure 3 | Comparing effective and instantaneous populations. a,**b**, Analysis of the relation between the dynamics of the effective (dashed) and instantaneous (solid) hole populations given by the TDCIS method for intensities of 2.0×10^{14} W cm^{-2} (**a**) and 3.2×10^{14} W cm^{-2} (**b**). The good qualitative agreement demonstrates the ability of the ATAS technique to track real-time—that is, instantaneous—SFI dynamics.

parameters—that is, the effective dipole strengths. The EHPs still exhibit the strong overshoots occurring at $2\omega_L$ frequency. Furthermore, two important features are established. First, the overshoots are stronger for the lower NIR intensity. Second, phase delays are observed experimentally between the hole dynamics from the two spin–orbit channels. At the lower intensity, the phase delays are negligible and the populations are almost in phase. However, at higher intensities the $5p_{3/2}^{-1}$ channel is clearly delayed with respect to the $5p_{1/2}^{-1}$ channel by approximately 200 as.

To better understand the mechanisms underlying the experimental observations, *ab initio* numerical calculations are performed simulating ATAS spectra in Xe under the experimental conditions (see Methods). The numerical calculations are based on the TDCIS method[21–23] and incorporate the effect of overlapping pump and probe pulses from first principles[24]. The same fitting procedure as mentioned above is then used to extract the EHP from the simulated ATAS spectra. These numerical reconstructions of the EHPs are shown in Fig. 2b. Both key features, the observation of overshoots as well as the trends in the oscillation strengths and phase delays between the two channels, are well reproduced by the TDCIS method. This comparison demonstrates that the TDCIS method is well suited to predict the SFI dynamics as observed in the experiment.

Comparing effective to instantaneous dynamics

After validating the theoretical model, we consider the analysis of the calculated effective hole dynamics extracted from ATAS. Within the oscillating dipole model, ATAS measures a signal over the lifetime of the core-hole—excited state; that is, a signal that is inherently non-local in time[30,31]. When the pump and probe pulses overlap in time, the intense NIR field after the probe step has been demonstrated to impart a phase shift to the oscillating dipole, which leads to the aforementioned line deformations[16,24,28]. Hence, it is highly non-trivial to assess whether or not this mechanism can also modify the effective dipole strengths and consequently cause a deviation of the EHP from the instantaneous values at the exact arrival time of the probe pulse.

To answer this question, we directly compare the aforeshown TDCIS EHP dynamics to the TDCIS instantaneous hole dynamics for the $5p_{1/2}^{-1}$ and $5p_{3/2}^{-1}$ channels in Fig. 3a,b for the intensities of 2.0×10^{14} and 3.2×10^{14} W cm^{-2}, respectively. The qualitative features of the instantaneous hole populations (IHPs), including the existence of overshoots and the depth of oscillations, match quite well with those of the EHPs. A phase delay is also consistently predicted between the spin–orbit states for the IHPs. Combining the results shown in Figs 2 and 3, the joint experimental and theoretical investigation provides evidence that ATAS in the case of overlapping pump and probe pulses is able to map out the essential features of the instantaneous strong-field valence-hole dynamics on the sub-fs time scale. Particularly, the overshoots observed in the effective hole dynamics are an intrinsic property of the SFI dynamics and are not an artificial product of the ATAS technique.

By tuning the Hamiltonian in the TDCIS calculations, it is found that many-electron correlations play only a minor role in the SFI process (see Supplementary Section 2.2). However, the long-range Coulomb ionic potential experienced by the excited electron has a vital impact on the SFI hole-creation process. In the absence of the long-range Coulomb tail, the ionization steps and the asymptotic ion yields for both channels are much smaller. Also, the delays of the overshoots are significantly underestimated (see Supplementary Section 2.3). The findings are in accordance with a previous numerical study[19], which shows that the commonly used SFI models, such as the standard strong-field approximation (SFA), are insufficient for the quantitative or even qualitative description of sub-cycle SFI dynamics.

Decomposing SFI dynamics: tunnelling and polarization

It is known that both adiabatic[1,25,26] and non-adiabatic[27] SFI theories predict ionization dynamics that grow monotonically in time. Hence, neither of the analytical models can account for the overshoots observed in the current study. To understand the origin of the overshoots, the instantaneous hole dynamics produced by pure tunnel ionization are computed on the basis of a CIS tunnelling rate calculation under the quasi-static approximation[32]. The results of the hole dynamics predicted by the tunnelling model are presented in Fig. 4a, in comparison with the TDCIS full quantum wavepacket calculations. Using the tunnelling dynamics as a baseline and subtracting it from the total TDCIS curve, a new type of strong-field behaviour is obtained, uniquely different from tunnel ionization. The differences between the TDCIS and tunnel ionization curves for various intensities are plotted in Fig. 4b and exhibit $2\omega_L$ oscillations in coarse synchrony with the square of the electric field $|\mathbf{E}(t)|^2$. The oscillations scale almost linearly with the peak field intensity $|\mathbf{E}_0|^2$, suggesting their origin is from the laser-induced dressing of the neutral ground state. In ref. 19, it is also shown that this perturbation acts to coherently mix the ground state with numerous excited and continuum states. Consequently, this effect is referred

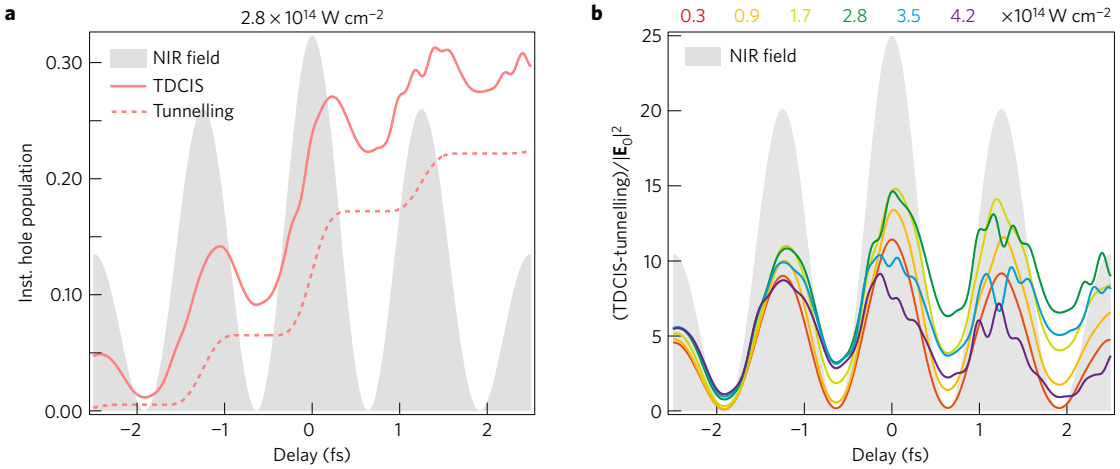

Figure 4 | Decomposing the strong-field dynamics. a, To investigate the origin of the oscillatory feature, tunnelling calculations are performed and plotted for $(j, m_j) = (1/2, 1/2)$ and an intensity of 2.8×10^{14} W cm^{-2}. **b**, Population differences between the full wavepacket calculation using TDCIS and the tunnelling calculations for various intensities normalized by the corresponding peak intensity $|\mathbf{E}_0|^2$. The linear dependence of the discrepancy between TDCIS and tunnelling substantiates the interpretation of the oscillatory feature as being a signature of a reversible electronic population or, more specifically, ground-state polarization.

to as ground-state polarization. This phenomenon reiterates the need for a long-range Coulomb potential between the strong-field-manipulated electron and the ion, since the Coulomb tail substantially increases the number of bound excited states in the atom, thus boosting the ground-state polarization process. Therefore, this combined experimental and theoretical study strongly suggests that, even in the presence of a strong laser field, the valence-hole creation can be created not only from the commonly expected irreversible tunnel mechanism, but also from a reversible polarization pathway. While the latter SFI process has been frequently overlooked in numerous theoretical[1,25–27] and experimental[2–5] works that focus exclusively on the asymptotic electron/ion production, it unambiguously manifests itself in hole production during the sub-cycle SFI dynamics revealed by the ATAS technique.

Having understood the origin of the overshoots in the ionization signal, we would like to discuss the origin behind the observed phase delay and the discrepancy between the experimentally and theoretically extracted values. Given that the ionization signal is composed of tunnelling and polarization, a trivial contribution dubbed apparent delay can be already identified as the phase delay created when the oscillatory signals (polarization) are added to two different tunnelling backgrounds (for example, different rise times between two plateaux). But, as can be seen from Fig. 4b, even after removing this contribution, the reversible hole dynamics and $|\mathbf{E}(t)|^2$ are not entirely synchronized. It is likely that this non-trivial delay is a signature of the non-adiabaticity in the SFI processes: in the adiabatic representation, both the tunnelling and polarization dynamics are decided by one single eigenstate that follows the instantaneous electric field strength. Under our experimental conditions, this picture is not entirely valid, and transitions among adiabatic eigenstates can take place at avoided crossings[32].

In addition, while the TDCIS method is well suited to predict the SFI dynamics as observed in the experiment, there are ultimately still a few limitations that can cause the discrepancies observed in this study. First, some higher-order correlation effects such as those involving double excitation are not included in the TDCIS method. Second, in the TDCIS approach applied here, relativistic effects (spin–orbit couplings) are included only for the hole orbitals on an *ad hoc* basis[24] and are entirely ignored for the photoelectron. Finally, we assume the Beer–Lambert law for the calculation of the XUV spectra. In reality, the two pulses involved may get significantly distorted during macroscopic propagation in the gas cell.

Wavepacket motion in the two limits

With the aid of theory, the experimentally observed real-time dynamics of SFI have been successfully identified as two competing mechanisms corresponding to tunnel ionization (irreversible) and bound electronic motion (reversible). To better visualize these contributions, we present calculated snapshots of the induced charge density of the wavepacket of Xe within a half-NIR cycle using the TDCIS method (see Supplementary Section 2.4). At low NIR intensities (Fig. 5a, $I = 0.3 \times 10^{14}$ W cm^{-2}), the hole-creation mechanism is governed by reversible ground-state dressing, which separates the positive and negative charges within the Xe atom. As the electron always stays close to the hole in this case, the wavefunction of the electron and that of the hole strongly interfere, forming rich and compact structures in the induced charge density. Close to the end of the half-cycle, the electron cloud flows back and fills in the hole, such that the hole population is restored to zero. At higher NIR intensities (Fig. 5b, $I = 3.2 \times 10^{14}$ W cm^{-2}), the dominant hole-creation mechanism is the irreversible tunnelling process. Starting from $-T/8$, the electric field quickly pulls the electron cloud away from the hole. The tunnel-ionized electron rapidly spreads out and disappears from the numerical box, leaving a permanent hole behind. The features in the wavepacket densities mainly arise from the individual contributions of the electron and the hole, while their interference does not play much of a role. In this irreversible hole-creation process, the hole population increases stepwise and monotonically during the NIR sub-cycle. For intermediate NIR intensities, as in most strong-field experiments, the hole-creation process is a mixture of the two mechanisms.

Discussion

With a better understanding of the sub-cycle features observed in SFI, it is now possible to place previous experiments concerning time-resolved strong-field ionization and excitation in the context of this work. In the pioneering experiment of Uiberacker *et al.*[12], tunnel ionization was observed by detecting the Ne^{2+} yield from shake-up states of Ne^+ that were populated by an attosecond XUV pulse. The authors observed 'dips' in the tunnel ionization steps that, however, were smaller than the error bars and could not be explained within their non-adiabatic tunnelling model. We believe that the occurrence of the dips in ref. 12 arises from a similar mechanism that accounts for the overshoots reported here: it is launched by strong NIR polarization of the Ne ground state, which subsequently

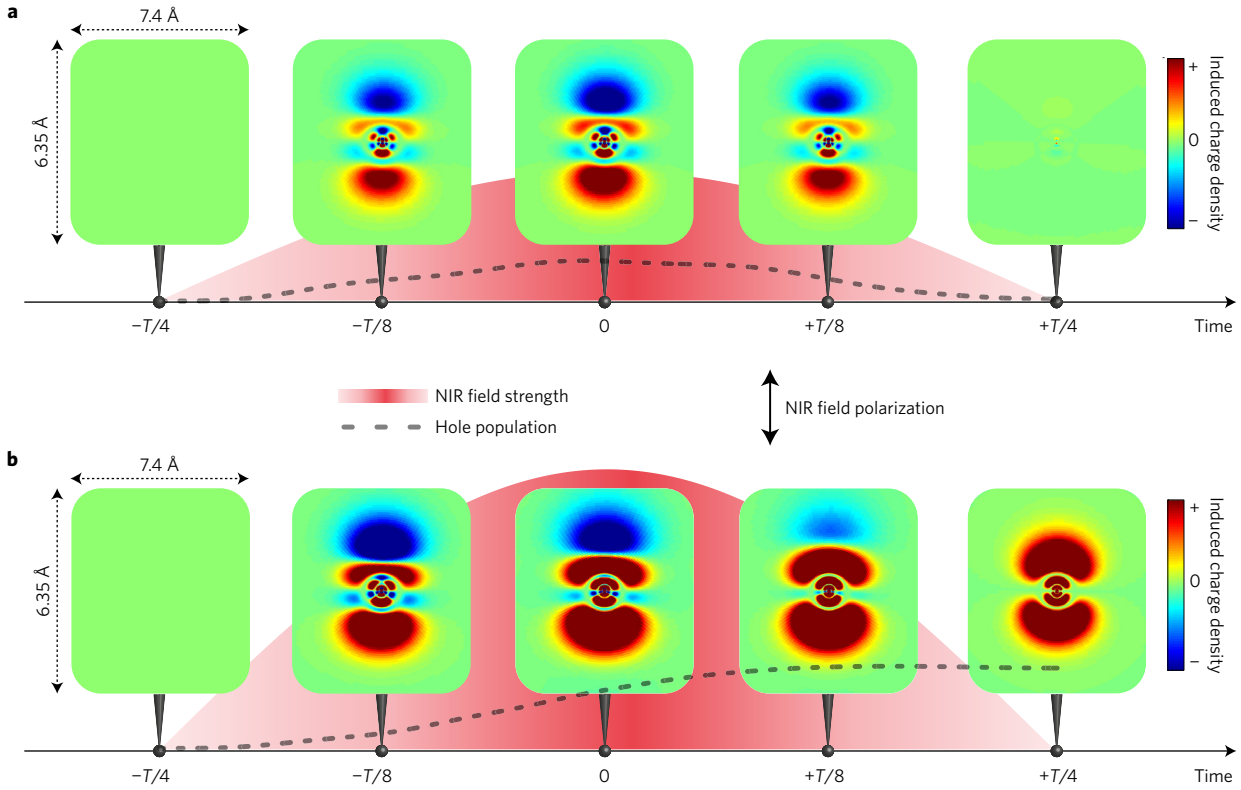

Figure 5 | Time evolution of the charge density induced in Xe by a strong laser field in different intensity regimes. The induced charge density is defined as the charge density of the driven wavepacket minus the charge density of the field-free ground state and is here depicted at five different instances in time within a half laser cycle $T/2$. **a**, Evolution for $I = 0.3 \times 10^{14}$ W cm^{-2}. Here, the dominant hole-creation process is given by ground-state polarization, which leads to reversible separation of positive and negative charges. When approaching the end of the half-cycle, the electron cloud flows back and fills in the hole—that is, the system relaxes back to its initial configuration. **b**, For higher NIR intensities ($I = 3.2 \times 10^{14}$ W cm^{-2}), the dynamics are dominated by irreversible processes governed by tunnel ionization. Hence, at the end of the half-cycle, the ground-state configuration has an irrecoverable loss, leaving a permanent hole behind.

modulates the shake-up process through electronic correlations. Later experiments observed strong-field excitation dynamics in solid-state fused silica and silicon. In fused silica, Schultze *et al.*[33] observed reversible $2\omega_L$ oscillations in synchrony with the electric field strength; however, in silicon, Schultze *et al.*[34] found distinct excitation steps with a periodicity of $2\omega_L$. The qualitative difference between the two experiments can be attributed to the bandgap of the material. Fused silica has a rather large bandgap of 9 eV, resulting in a higher Keldysh parameter than the 3.2 eV bandgap of silicon. As a result, driving fused silica with a strong electric field gave rise to a polarization response between conduction and valence bands, while subjecting silicon to the same electric field strengths results in irreversible charge carrier excitation.

Although this study provides an intuitive understanding of sub-cycle features in strong-field ionization, further investigations need to be taken to shed light onto the non-trivial origin of the observed phase delay. The large ground-state polarization of heavy elements and molecules will help to achieve this goal. Furthermore, taking advantage of the state specificity of the ATAS technique, we anticipate the extension of our method to the real-time observation of strong-field-induced ultrafast charge migration[31,35–37].

Methods

Methods, including statements of data availability and any associated accession codes and references, are available in the online version of this paper.

Received 1 August 2016; accepted 3 January 2017; published online 6 February 2017

References

1. Keldysh, L. V. Ionization in the field of a strong electromagnetic wave. *Sov. Phys. JETP* **20,** 1307–1314 (1965).
2. Voronov, G. S. & Delone, N. B. Many-photon ionization of the xenon atom by ruby laser radiation. *Sov. Phys. JETP* **23,** 54–58 (1966).
3. Chin, S. L., Yergeau, F. & Lavigne, P. Tunnel ionisation of Xe in an ultra-intense CO_2 laser field (10^{14} W cm^{-2}) with multiple charge creation. *J. Phys. B* **18,** L213 (1985).
4. Augst, S., Meyerhofer, D. D., Strickland, D. & Chin, S. L. Laser ionization of noble gases by Coulomb-barrier suppression. *J. Opt. Soc. Am. B* **8,** 858–867 (1991).
5. Monot, P., Auguste, T., Lompré, L. A., Mainfray, G. & Manus, C. Focusing limits of a terawatt laser in an underdense plasma. *J. Opt. Soc. Am. B* **9,** 1579–1584 (1992).
6. Drescher, M. *et al*. Time-resolved atomic inner-shell spectroscopy. *Nature* **419,** 803–807 (2002).
7. Cavalieri, A. L. *et al*. Attosecond spectroscopy in condensed matter. *Nature* **449,** 1029–1032 (2007).
8. Neppl, S. *et al*. Attosecond time-resolved photoemission from core and valence states in magnesium. *Phys. Rev. Lett.* **109,** 087401 (2012).
9. Schultze, M. *et al*. Delay in photoemission. *Science* **328,** 1658–1662 (2010).
10. Klünder, K. *et al*. Probing single-photon ionization on the attosecond time scale. *Phys. Rev. Lett.* **106,** 143002 (2011).
11. Sabbar, M. *et al*. Resonance effects in photoemission time delays. *Phys. Rev. Lett.* **115,** 133001 (2015).
12. Uiberacker, M. *et al*. Attosecond real-time observation of electron tunnelling in atoms. *Nature* **446,** 627–632 (2007).
13. Goulielmakis, E. *et al*. Real-time observation of valence electron motion. *Nature* **466,** 739–743 (2010).
14. Wang, H. *et al*. Attosecond time-resolved autoionization of argon. *Phys. Rev. Lett.* **105,** 143002 (2010).
15. Holler, M., Schapper, F., Gallmann, L. & Keller, U. Attosecond electron wave-packet interference observed by transient absorption. *Phys. Rev. Lett.* **106,** 123601 (2011).

16. Wirth, A. *et al*. Synthesized light transients. *Science* **334,** 195–200 (2011).
17. Dalgarno, A. & Kingston, A. E. The refractive indices and Verdet constants of the inert gases. *Proc. R. Soc. Lond. A* **259,** 424–431 (1960).
18. Langhoff, P. W. & Karplus, M. Padé summation of the Cauchy dispersion equation. *J. Opt. Soc. Am.* **59,** 863–871 (1969).
19. Smirnova, O., Spanner, M. & Ivanov, M. Coulomb and polarization effects in sub-cycle dynamics of strong-field ionization. *J. Phys. B* **39,** S307 (2006).
20. Dimitrovski, D. & Madsen, L. B. Time dependence of ionization and excitation by few-cycle laser pulses. *Phys. Rev. A* **78,** 043424 (2008).
21. Greenman, L. *et al*. Implementation of the time-dependent configuration-interaction singles method for atomic strong-field processes. *Phys. Rev. A* **82,** 023406 (2010).
22. Rohringer, N., Gordon, A. & Santra, R. Configuration-interaction-based time-dependent orbital approach for *ab initio* treatment of electronic dynamics in a strong optical laser field. *Phys. Rev. A* **74,** 043420 (2006).
23. Pabst, S., Greenman, L., Mazziotti, D. A. & Santra, R. Impact of multichannel and multipole effects on the Cooper minimum in the high-order-harmonic spectrum of argon. *Phys. Rev. A* **85,** 023411 (2012).
24. Pabst, S. *et al*. Theory of attosecond transient-absorption spectroscopy of krypton for overlapping pump and probe pulses. *Phys. Rev. A* **86,** 063411 (2012).
25. Perelomov, A. M., Popov, V. S. & Terent'ev, M. V. Ionization of atoms in an alternating electric field. *Sov. Phys. JETP* **23,** 924–934 (1966).
26. Ammosov, M. V., Delone, N. B. & Krainov, V. P. Tunnel ionization of complex atoms and of atomic ions in an alternating electromagnetic field. *Sov. Phys. JETP* **64,** 1191–1194 (1986).
27. Yudin, G. L. & Ivanov, M. Y. Nonadiabatic tunnel ionization: looking inside a laser cycle. *Phys. Rev. A* **64,** 013409 (2001).
28. Ott, C. *et al*. Lorentz meets Fano in spectral line shapes: a universal phase and its laser control. *Science* **340,** 716–720 (2013).
29. Jurvansuu, M., Kivimäki, A. & Aksela, S. Inherent lifetime widths of Ar $2p^{-1}$, Kr $3d^{-1}$, Xe $3d^{-1}$, and Xe $4d^{-1}$ states. *Phys. Rev. A* **64,** 012502 (2001).
30. Santra, R., Yakovlev, V. S., Pfeifer, T. & Loh, Z.-H. Theory of attosecond transient absorption spectroscopy of strong-field-generated ions. *Phys. Rev. A* **83,** 033405 (2011).
31. Leone, S. R. *et al*. What will it take to observe processes in 'real time'. *Nat. Photon.* **8,** 162–166 (2014).
32. Karamatskou, A., Pabst, S. & Santra, R. Adiabaticity and diabaticity in strong-field ionization. *Phys. Rev. A* **87,** 043422 (2013).
33. Schultze, M. *et al*. Controlling dielectrics with the electric field of light. *Nature* **493,** 75–78 (2013).
34. Schultze, M. *et al*. Attosecond band-gap dynamics in silicon. *Science* **346,** 1348–1352 (2014).
35. Cederbaum, L. S. & Zobeley, J. Ultrafast charge migration by electron correlation. *Chem. Phys. Lett.* **307,** 205–210 (1999).
36. Breidbach, J. & Cederbaum, L. S. Migration of holes: formalism, mechanisms, and illustrative applications. *J. Chem. Phys.* **118,** 3983–3996 (2003).
37. Kraus, P. M. *et al*. Measurement and laser control of attosecond charge migration in ionized iodoacetylene. *Science* **350,** 790–795 (2015).

Acknowledgements

This material is based upon work supported by the National Science Foundation (NSF) (CHE-1361226) and the US Army Research Office (ARO) (W911NF-14-1-0383). Z.-H.L. acknowledges support from the Ministry of Education (MOE2014-T2-2-052) and the Agency for Science, Technology and Research (1223600008 and 1321202083). S.P. is funded by the Alexander von Humboldt Foundation and by the NSF through a grant to ITAMP.

Author contributions

M.S. and H.T. performed the experiment and the data analysis. M.S., H.T., Z.-H.L., A.K.P. and S.G.S. designed and implemented the experimental set-up. Y.-J.C. conducted theoretical modelling, supported by S.P. and supervised by R.S. M.S., H.T. and Y.-J.C. wrote the manuscript, with input from all authors. The project was supervised by S.R.L.

Additional information

Supplementary information is available in the online version of the paper. Reprints and permissions information is available online at www.nature.com/reprints. Correspondence and requests for materials should be addressed to M.S. or S.R.L.

Competing financial interests

The authors declare no competing financial interests.

Methods

Experimental approach. Attosecond XUV pulses are generated by means of high-harmonic generation in argon. For the proper isolation of a single sub-200 as pulse, the recently developed PASSAGE[38] technique is applied. The attosecond pulse is spatially and temporally overlapped with an intense few-cycle NIR laser pulse in an interferometric scheme that allows the precise control of the delay between the two pulses with a long-term accuracy of 80 as r.m.s. A toroidal mirror is subsequently used to focus both pulses into a Xe-filled gas cell. The SFI induced by the NIR laser pulse is probed via absorption of the delayed attosecond pulse using an XUV photon spectrometer. For further details of the experimental set-up, please refer to the Supplementary Information.

Theoretical approach. The attosecond transient absorption spectra of atomic Xe and the effective hole dynamics thereof are obtained by numerical solutions of the N-electron time-dependent Schrödinger equation (TDSE) within the framework of TDCIS using our XCID package[39]. TDCIS is an *ab initio* electronic-structure theory that is able to capture essential electronic correlation effects beyond the mean-field level[21–23], and has been successfully applied to study diverse strong-field processes[40], including ATAS[16,24]. For each pump–probe delay, the TDCIS wavepacket is computed for an electric field profile containing the overlapping NIR pump and XUV probe. This explicitly takes into account the non-perturbative nature of the pump pulse. The ATAS spectrum measured at the detector is constructed by Gaussian-convoluted Fourier transformation of the time-dependent ionic dipole moment assuming the Beer–Lambert law[24,30].

The full instantaneous hole dynamics are calculated by solving the TDSE within TDCIS under the sole influence of the pump[21]. For the tunnelling hole dynamics, the tunnelling rates for each $5p_{j,m_j}$ channel at different instantaneous NIR intensities are acquired by numerical diagonalization of the CIS Hamiltonian subjected to a complex absorbing potential under the quasi-static approximation[41,42]. The tunnelling rates at various d.c. field strengths are then fed into rate equations to predict the IHPs due to the irreversible tunnelling mechanism.

Data availability. All data that support the plots within this paper and other findings of this study are available from the corresponding authors upon reasonable request.

References

38. Timmers, H. *et al*. Polarization-assisted amplitude gating as a route to tunable, high-contrast attosecond pulses. *Optica* **3,** 707–710 (2016).
39. Pabst, S. *et al*. *XCID–The Configuration-Interaction Dynamics Package* Rev. 1220 (CFEL, DESY, 2014).
40. Pabst, S. Atomic and molecular dynamics triggered by ultrashort light pulses on the atto-to picosecond time scale. *Eur. Phys. J.* **221,** 1–71 (2013).
41. Chen, Y.-J., Pabst, S., Karamatskou, A. & Santra, R. Theoretical characterization of the collective resonance states underlying the xenon giant dipole resonance. *Phys. Rev. A* **91,** 032503 (2015).
42. Santra, R., Dunford, R. W. & Young, L. Spin–orbit effect on strong-field ionization of krypton. *Phys. Rev. A* **74,** 043403 (2006).